Noise reduction in qubit readout with a two-mode squeezed interferometer

G. Liu†, X. Cao†, T.-C. Chien, C. Zhou, P. Lu, and M. Hatridge*
Department of Physics and Astronomy, University of Pittsburgh, Pittsburgh, Pennsylvania 15260, USA
(Dated: August 25, 2020)

Abstract Fault-tolerant quantum information processing with flawed qubits and gates requires highly efficient, quantum non-demolition (QND) qubit readout. In superconducting circuits, qubit readout using coherent light with fidelity above 99% has been achieved by using quantum-limited parametric amplifiers such as the Josephson Parametric Converter (JPC). However, further improvement of such measurement is fundamentally limited by the vacuum fluctuations of the coherent light used for readout. In this work we measure a transmon qubit/cavity system with an unbalanced two-mode squeezed light interferometer formed from two JPCs. The first amplifier generates two-mode squeezed vacuum at its output, which is coherently recombined by the second amplifier after one branch is shifted and displaced by the transmon's state after it interacts with the qubit/cavity system on one arm of the interferometer. We have observed a 44% improvement in power Signal-to-Noise Ratio (SNR) of projective readout compared to that of coherent light readout in the same system. To investigate the quantum properties of the two-mode squeezed light in the system, we also studied weak measurement and found, surprisingly, that tuning the interferometer to be as unprojective as possible was associated with an increase in the quantum efficiency of our readout relative to the optimum setting for projective measurement. These enhancements may enable remote entanglement with lower efficiency components in a system with qubits in both arms of the interferometer.

I. INTRODUCTION

Measurement is the act by which we gain information about a quantum object (in quantum information processing usually a qubit) we wish to study. Although the end result of a measurement is classical information on our qubit, the measurement apparatus itself is comprised of three important components[1]. The first is the interaction between the information 'carrier' and the qubit to be measured. For superconducting qubits, this is almost universally the interaction between the probe signal and a dispersively coupled system formed by a microwave qubit to a microwave cavity, in which the cavity's frequency is shifted by photon number in the qubit [2]. The second component is the nature of the information carrier. Typically, this is coherent pulse of microwave light which we can think of as a flying coherent state. This pulse is sent into the cavity, where it experiences (for concreteness in a reflection experiment) a qubit-state-dependent phase shift due to the dispersive coupling [1]. The third component is the device which processes quantum information carrier so that it can be digitized at room temperature. In a typical circuit QED experiment, this is usually a Josephson junction based parametric amplifier [3–6].

For use in quantum information processing, where error correction and state preparation are paramount goals, the measurement should also be QND, that is the qubit state should not suffer additional back-action or randomization during the measurement process[7] . In circuit QED this requirement is satisfied by the dispersive qubit-cavity interaction, provided the readout pulse is not too strong [8, 9].

A 'good' measurement apparatus allows the experimenter to use the classical outcome of the measurement process to distinguish the qubit's state with high fidelity from a single measurement. For measurements based on (Gaussian) coherent pulses of light processed with either a phase-preserving or phase-sensitive amplifier (the workhorses of circuit QED [10–12]), the distinguishability is given by how far apart the Gaussian distributions of the measurement outcomes received at room temperature are. If the amplifiers are quantum limited [13], the ultimate limit on how large the readout pulse must be, and therefore how hard the cavity must be driven in order to reach a target SNR for a measurement, are the quantum fluctuations inherent in coherent states of light.

In this work, we demonstrate the use of two-mode squeezed (TMS) light and phase-preserving amplifier combined into an interferometer for dispersive qubit readout, as proposed in Ref. [14]. This measurement scheme is based on a Mach-Zehnder interferometer with active non-linear beam splitters which is commonly known as a SU(1,1) interferometer [15]. Two-mode squeezed light naturally forms a pair of Gaussian, entangled states which travel along two paths, and when recombined in a phase-preserving amplifier, which in the quantum limit naturally has two input and output ports [4, 16, 17], can achieve superior readout SNR (and hence fidelity) by lowering the output noise level through the destructive interference between the two modes. We take advantage of the fact that two-mode squeezing and phase-preserving amplification are the same process, using two nominally identical, single-ended Josephson Parametric Converters (JPCs) to generate and process two-mode squeezed light [4, 18, 19] in the interferometer. The qubit-cavity system is embedded in one arm of the interferometer, where it imbalances the system by imparting a qubit-state dependent phase shift on light

* hatridge@pitt.edu; † these authors contributed equally

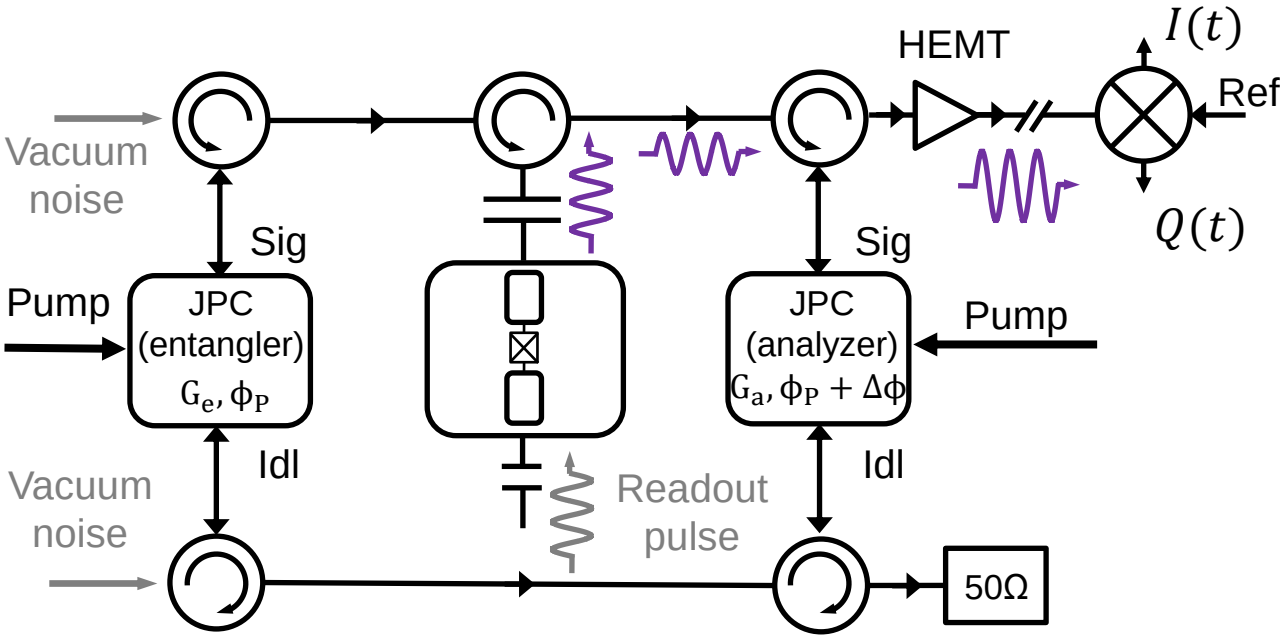

FIG. 1. **Schematic of the experiment setup.** Two nominally identical JPCs, entangler and analyzer, are connected by their signal (Sig) and idler (Idl) ports respectively with circulators and superconducting cables to form an interferometer. The unused ports on the circulators are terminated in cold 50 Ω loads which provide quantum vacuum noise to the entangler, and a dump for the unused signal on the lower arm of the interferometer. The upper arm of the interferometer is interrupted by a 3D transmon qubit-cavity system. The qubit measurement pulse is sent into the cavity via its weakly coupled port without going through both arms of the interferometer which enables the switching between the two-mode squeezed light readout and coherent light readout *in situ* by turning on and off the pump of the entangler JPC. The signal is subsequently further amplified by a cryogenic HEMT and demodulated and recorded at room temperature.

passing through that arm. To allow fair comparison with standard coherent pulse readout, we perform readout by a combination of TMS vacuum and a cavity displacement drive which enters the system through the cavity's weakly coupled port, and so is subjected to no interference effects. Thus, our overall readout scheme has fixed measurement strength and gain (20 dB), and only the noise is affected by introduction of TMS light.

For most settings, the readout produces unequal, state-dependent noise, so that the amplifier's output noise, even in the absence of the cavity displacement drive, can (poorly) read out the qubit, resulting in unwanted qubit dephasing whenever the amplifiers are active. There are, however, two particular settings for which the output noise powers match. In one which we term the 'low-match point', the output noise is suppressed below the standard quantum limit by the destructive interference between the correlated TMS noise entering the JPC [16, 20], resulting in a 44 % improvement in power SNR comparing to coherent light readout. As readout fidelity scales exponentially with SNR, this improvement could result in substantial increases in measurement fidelity for quantum information processing. The second, 'high-match point' has significantly larger noise than coherent light readout, with an associated degradation in SNR, and so is not helpful for projective readout.

However, the picture changes when we use weak measurements to characterize the quantum efficiency of our TMS light measurements. This calibration technique [12], which has well-known predictions for coherent state inputs with either phase-sensitive or phase-preserving amplification, uses the purely quantum phase back-action of measurement on the qubit to provide an unambiguous measure of what fraction the information in the readout pulse reaches the observer. An efficiency $\eta = 1$ resulting in fully trackable qubit evolution for either amplifier, though optimal phase-sensitive amplification has twice the SNR in projective measurement [21]. We applied this protocol to the TMS light readout with low- and high-match conditions, and found, to our surprise, that the observed efficiency varied inversely with SNR, that is the low-match point produced superior SNR together with a far less trackable phase back-action, and vise versa for the high-match point.

While we lack a detailed theory to explain this effect, it has important implications. Protocols which use measurement to generate entanglement via measurement of two remote qubits[22–25] rely on projecting the two qubits into a definite parity manifold while not scrambling the phase of states within that manifold. Thus the TMS readout at the high-match setting, which can readily accommodate a second qubit on the other arm, could

allow remote entanglement to succeed in the presence of flawed components by flexibly rebalancing the trade-off between projectivity and phase-scrambling *in situ*.

II. EXPERIMENT SETUP

In our experiment the two-mode squeezed light is generated, analyzed and amplified with JPCs (Fig. 1). A JPC is a non-degenerate phase-preserving amplifier based on the three-wave mixing process in a ring of four nominally identical Josephson junctions, known as a Josephson Ring Modulator (JRM). The JPC's Hamiltonian can be written as [4, 18]:

$$\frac{H_{JPC}}{\hbar} = \omega_a a^\dagger a + \omega_b b^\dagger b + \omega_c c^\dagger c + g_3(a^\dagger b^\dagger c + abc^\dagger), \quad (1)$$

where a, b, and c are the annihilation operators of the three modes of the JPC which are refereed to as 'signal', 'idler', and 'common' mode respectively, and g_3 is the three-wave coupling strength. Phase-preserving amplification is achieved by applying a strong microwave drive to the common mode at frequency $\omega_p \simeq \omega_a + \omega_b$. When ω_p is far detuned from ω_c, the pump is 'stiff' in the sense that c can be replaced by its average value $\langle c \rangle e^{i\phi_p}$, where $\langle c \rangle$ and ϕ_p are the pump amplitude and phase, respectively. This reduces the three-wave mixing term to an effective two-wave coupling term between the signal and idler mode: $g_3 \langle c \rangle (e^{i\phi_p} a^\dagger b^\dagger + e^{-i\phi_p} ab)$. As an amplifier, this device amplifies signals in reflection with amplitude gain of $\sqrt{G}$, and in transmission with frequency conversion and amplitude gain of $e^{i\phi_p}\sqrt{G-1}$. The same two-mode Hamiltonian can also be described by the two-mode squeezing operator [26]: $S = \exp(re^{-i\phi_p} ab - re^{i\phi_p} a^\dagger b^\dagger)$, where $re^{i\phi_p}$ is the complex squeezing parameter with $r = \cosh^{-1}\sqrt{G}$ [27, 28]. Thus, the JPC, or any other non-degenerate phase-preserving amplifier, can also serve as a generator of two-mode squeezed light with both spectral and spacial non-degeneracy [19, 29].

In our experiment, we form an active interferometer with two nominally identical JPCs, the 'entangler' and 'analyzer', by connecting their signal and idler ports [19] (Fig. 1). Uncorrelated vacuum noise enters the interferometer via the inputs of the entangler JPC, which transforms them into highly correlated, two-mode squeezed vacuum traveling along the two arms of the interferometer. These two paths recombine and interfere with each other in the analyzer JPC, generating outputs controlled by the gains and relative pump phase of the two JPCs. The input is doubly amplified with zero relative pump phase between the two JPCs (yielding a net amplifier with power gain $G_e G_a$), while a π relative pump phase will cause the analyzer JPC to de-amplify the output of the entangler JPC. In the absence of loss and added noise, the output of the interferometer will return to uncorrelated vacuum if the gains of the two JPCs are matched and their pump phases are different by π.

We use the interferometer to read out a qubit by interrupting the upper arm with a microwave cavity, which in turn is dispersively coupled to a transmon qubit, as shown in Fig. 1. To achieve a better SNR than qubit readout with coherent light input and phase-preserving amplification (CS + PP), the dispersive phase shift due to interaction with the qubit-cavity system must be either close to zero or π, which correspond to the qubit-cavity dispersive shift χ being much smaller or larger than the cavity linewidth κ [14]. In our experiment, we design the quit-cavity system to be in the small dispersive shift regime with $\chi/\kappa = 0.22$ which is favorable for fast readout (see supplementary for the parameters of the experiment).

Although the noise of the interferometer itself can read out the qubit for many combinations of entangler and analyzer gain and relative phase, high SNR readout requires a coherent drive to be applied to the system. The original proposal called for displacing the input to the upper arm of the entangler [14], however in this scenario the signal is both amplified and partially transmitted down both arms of the interferometer, so that there is interference in both the output signal and noise. This greatly complicates fair comparison with CS + PP readout, and so in our experiment we drive our readout through a second, weakly coupled port in the microwave cavity. The readout signal thus does not interfere, and experiences the same gain (from the analyzer only) in both our TMS and CS + PP readout. In this case, we squeeze only on the noise, with a degredation/enhancement of SNR corresponding to a larger/smaller output noise, respectively.

III. RESULTS

A. Generation of two-mode squeezed vacuum

As a first step towards qubit readout with two-mode squeezed light, we demonstrate in Fig. 2 the signatures of coherent interference between the two parts of the two-mode squeezed vacuum generated by the entangler. We measure the output noise voltage at the signal port of the analyzer while sweeping the relative phase ($\Delta\phi$) between the two pump tones for different squeezing strength, G_e, on the entangler JPC. The gain of the analyzer JPC, G_a, is kept constant at 20 dB. For each shot of the measurement, the qubit is prepared in the ground state by post-selecting the result of an initial, projective measurement. After initializing the qubit state, we wait for 10 cavity lifetimes before recording the output voltage of the system for a 660 ns period, from which we obtain the quadrature voltage values (I_m, Q_m) of the noise. For a given squeezing strength, at each relative pump phase, the same measurement is repeated 50,000 times and the outcomes are plotted in the form of a 2D histogram. Fig. 2(a) shows the line cuts along $Q_m = 0$ of the 2D histograms of the measurement outcomes with the entangler off, $G_e = 0$ dB (CS + PP), versus entangler on

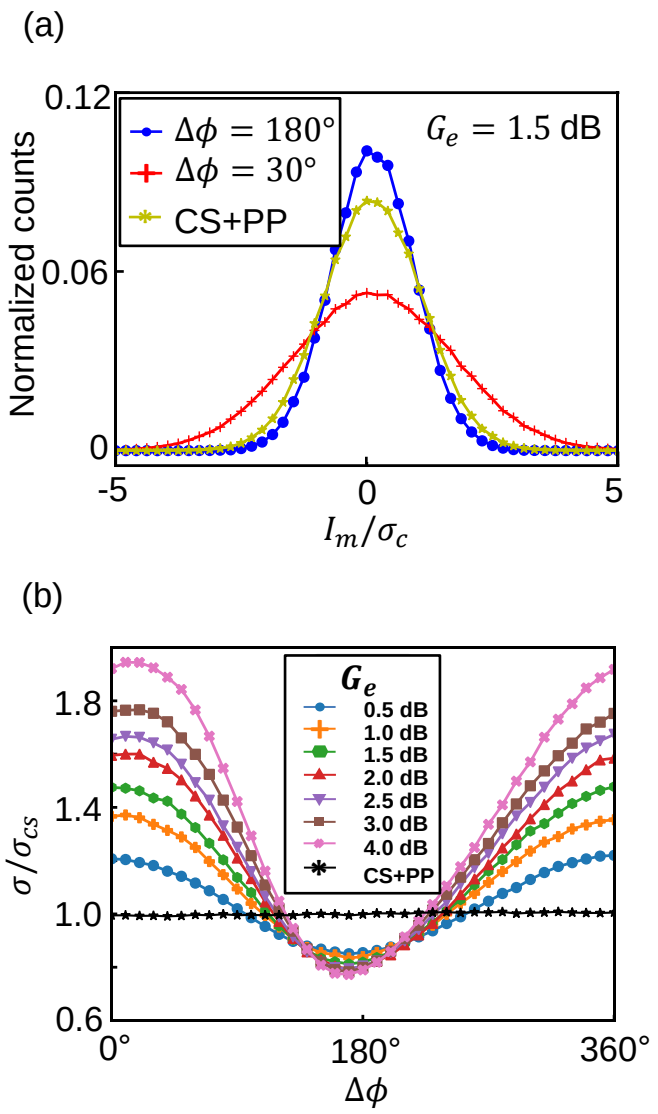

FIG. 2. **Two-mode squeezed vacuum.** (a) Normalized 1D Gaussian distribution of noise measurement result for the two-mode squeezed vacuum at featured relative pump phase point with a $G_e = 1.5$ dB. The red cross and blue dot curves are obtained by applying a line cut along $Q_m = 0$ of the 2D histograms at relative pump phase point that gives the highest and lowest noise level respectively. The curve for the case of coherent light (yellow star) is also shown for comparison. (b) Normalized standard deviation of output noise voltage of two-mode squeezed vacuum as a function of relative pump phase $\Delta\phi$ at different entangler gain G_e. The standard deviation of noise voltage at each relative pump phase and entangler gain is obtained by fitting a histograms of 50, 000 repeated measurement results (see supplementary) to a 2D Gaussian distribution. The black star line shows the noise level of the coherent vacuum input as a reference while the other colors each represents a different gain for the entangler JPC. During the measurement, the analyzer gain is $G_a = 20$ dB.

with $G_e = 1.5$ dB at two different relative pump phases. All the curves are normalized so that the area under the curve is 1. Comparing to the unsqueezed input (CS + PP), the output noise voltage of the two-mode squeezed vacuum changes from larger to smaller than that of the amplified vacuum as the two pumps go from in phase to out phase with each other, which demonstrates the correlation between the two parts of the two-mode squeezed vacuum traveling on the two arms of the interferometer.

By fitting the histogram to a 2D Gaussian distribution, the standard deviation of the measurement outcome (σ_I, σ_Q) can be extracted. In Fig. 2(b) we plot the standard deviations of the noise measurement outcomes with respect to relative pump phase for entangler gain ranging from 0 dB to 4 dB (as $\sigma_I \simeq \sigma_Q$ we plot their average). For easier comparison, all the data shown in this figure are normalized by the average standard deviation of the measurement outcome of $G_e = 0$ dB, which is the noise for standard CS + PP qubit measurement. We can see that the output noise level of the two-mode squeezed vacuum oscillates with the relative pump phase. In particular, there exists a range of relative pump phase within which it goes below that of the amplified unsqueezed vacuum. This oscillatory pattern clearly shows the existence of coherent interference between photons in the two arms of the interferometer. It also shows that the output noise level of the two-mode squeezed vacuum can be controlled by the relative pump phase. As the gain of the entangler increases, the suppression of the noise becomes stronger, but at the same time the phase range for noise suppression becomes smaller. This sets the limit for SNR improvement attainable in a given qubit-cavity system. We note that similar result has previously been observed in a setup with only two JPCs and no qubit [19].

B. Qubit readout with two-mode squeezed vacuum

In order to utilize the two-mode squeezed vacuum for qubit readout, we first study the effect of the dispersive qubit-cavity phase shift on the interferometer. To do so, we repeat the measurements from Fig. 2 with $G_e = 2.0$ dB and the qubit now being prepared either in the ground or excited state, and the results are shown in Fig. 3(a). The noise behavior of two-mode squeezed vacuum for qubit in ground and excited states are very similar, with a relative phase shift of 40° which is due to the qubit-state dependent dispersive phase shift on photons traveling on the upper arm of the interferometer. For a given relative pump phase, this extra phase shift creates a qubit-state dependent output noise power. This means that, except for the two relative phases ($\Delta\phi = 190°$ and 330°) where the output noise is identical for both qubit states , the noise of the interferometer can measure/dephase the qubit state without any input drive applied to the cavity. This is very different from CS + PP readout where the cavity must be driven to perform measurement, and the amplifier being on or off should

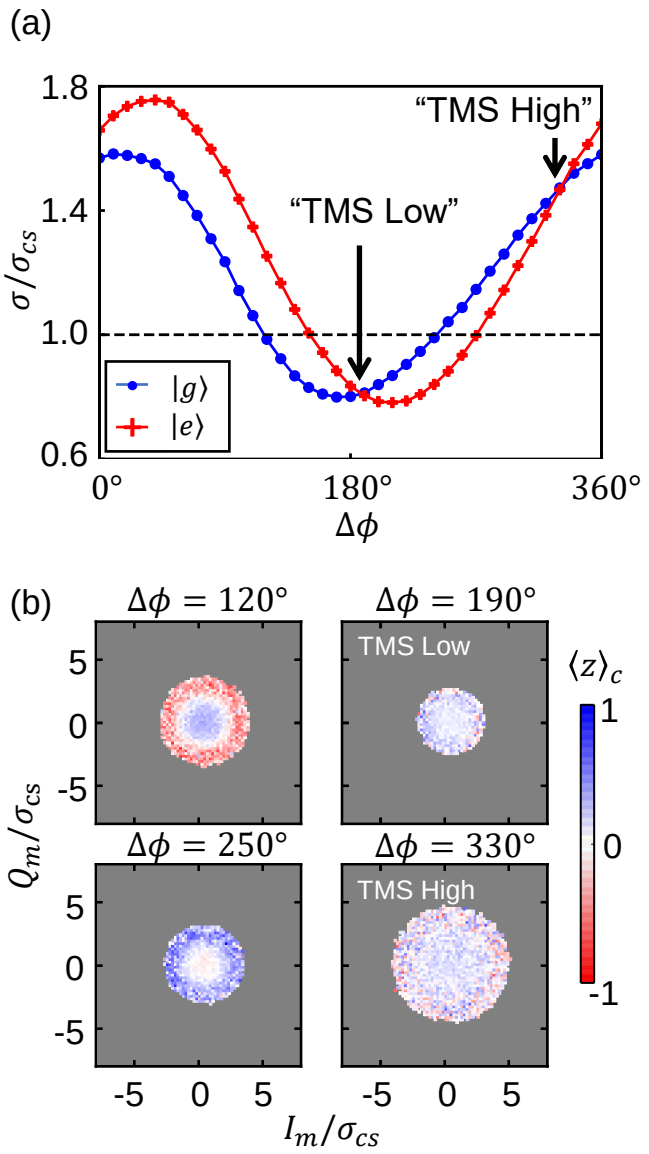

FIG. 3. **Qubit readout with two-mode squeezed vacuum.** (a) Normalized standard deviation of output noise voltage for two-mode squeezed vacuum input on the analyzer as a function of relative pump phase and qubit state. The black dotted line shows the standard deviation when the input of the analyzer is the coherent (unsqueezed) vacuum. Blue and red curves represent results for two-mode squeezed vacuum noise recorded when the qubit is in $|g\rangle$ and $|e\rangle$ state respectively. (b) Conditional tomography data for the z component of the qubit Bloch vector after we record the output noise for 660 ns at different relative pump phases. The qubit is prepared in the state of $(|g\rangle + i\,|e\rangle)/\sqrt{2}$. The entangler gain is $G_e = 2.0$ dB and the analyzer gain is $G_a = 20$ dB.

not affect the qubit's dephasing rate.

To demonstrate this 'two-mode squeezed vacuum' readout in the interferometer, we modify our measurement protocol by changing the initial state of the qubit to $(|g\rangle + i\,|e\rangle)/\sqrt{2}$, and adding a strong measurement after recording the noise output voltage to determine the final state of the qubit. As in References [12, 22], we construct a histogram where each pixel contains the average of all final measurement results of the z-component of the qubit state Bloch vector conditioned on receiving a particular (I_m,Q_m) voltage in the second (noise) measurement. Fig. 3(b) shows these conditional z-axis tomography results at four different relative pump phases: $\Delta\phi = 120°$ and $250°$, at which the difference between the output noise power for qubit in ground and excited state is the largest, and $\Delta\phi = 190°$ and $330°$ at which the output noise power for qubit in ground and excited state are the same. At $\Delta\phi = 120°$, we clearly see a 'Bullseye' pattern, with the qubit found to be in $|e\rangle$ if the recorded noise voltage is large, and in $|g\rangle$ if the recorded noise voltage is small. A similar result is also seen at $\Delta\phi = 250°$, with the correspondence between the noise voltage amplitude and qubit state reversed. These results show that two-mode squeezed vacuum in our inteferometer, unlike unsqueezed vacuum, can entangle with the qubit state. An observer with a power meter could perform a (poor fidelity) readout of the qubit simply by measuring how much noise the circuit emits. This also implies that powering the entangler and analyzer will generate continuous qubit dephasing for these bias points. In contrast, at $\Delta\phi = 190°$ and $330°$ where the output noise levels are the same for different qubit states, and so, similarly to unsqueezed vacuum, no information about the qubit can be inferred from the circuit's noise output. We will focus in the next two sections of this paper on experiments at the two 'matched' noise points, which we refer to as 'TMS High' and 'TMS Low' for the point with larger and smaller matched noise, respectively.

C. SNR improvement with displaced two-mode squeezed vacuum

In standard dispersive qubit readout, a coherent microwave pulse containing several photons is used to extract the qubit state information [12, 30]. We are now going to show that SNR of such measurements can be improved by replacing the coherent light with two-mode squeezed light of the same strength. The SNR in our experiment is defined as:

$$\mathrm{SNR} = \frac{(I_c^g - I_c^e)^2 + (Q_c^g - Q_c^e)^2}{\sigma_g^2 + \sigma_e^2} \tag{2}$$

where $(I_c^{g(e)}, Q_c^{g(e)})$ is the center of the measurement result distribution when the qubit is in ground (excited) state and $\sigma_{g(e)}$ is the corresponding standard deviation. To determine the SNR, we prepare the qubit in the ground and excited state separately, and then perform the readout by sending a coherent probe signal through the cavity from its weak port. Given that the coupling strength of the strong port is much greater than that of the weak port ($Q_{weak} \gg Q_{strong}$), quantum fluctuation of the field inside the cavity will be set by the two-mode

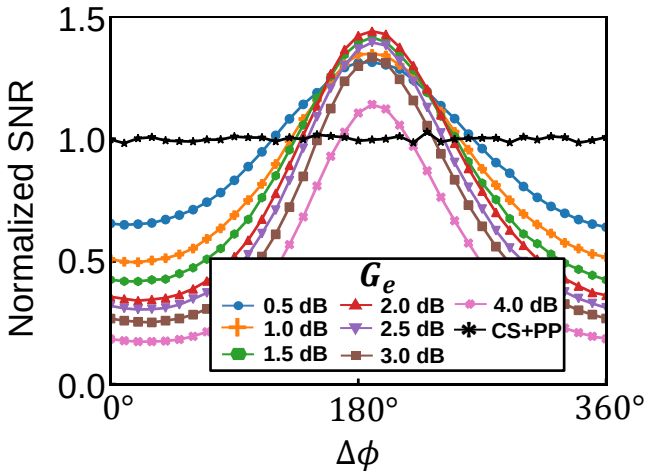

FIG. 4. **SNR of qubit readout with coherent light and displaced two-mode squeezed vacuum.** Normalized power SNR for qubit readout with coherent light, and with displaced two-mode squeezed vacuum at different squeezing strength (G_e) as a function of relative pump phase. The SNR is calculated according to Eq. 2 where the parameters are extracted from a 2D Gaussian fitting of the corresponding data.

squeezed vacuum present at the strong port. For fair comparison with standard CS + PP readout, we drive the system from the weak port in all cases, rather than driving the entangler amplifier as proposed in [14]. This has the advantage that there is ideally no interference in the amplitude of our signals, and a uniform displacement of the cavity in all measurements (see Fig. S.4), and so any change in SNR will be solely due to changing the quantum noise in the interferometer, rather than larger or smaller displacements drives applied to the cavity.

In Fig. 4, we show the SNR of the dispersive readout with displaced two-mode squeezed vacuum as a function of relative pump phase for different entangler gain. The data is normalized to the average SNR of coherent light ($G_e = 0$ dB) readout with the same strength. Improvement in SNR, as large as 44%, is observed for relative pump phase in the range of 140° to 240° over a wide range of entangler gain. In this range, the signal is actually 8% *smaller* than in CS+PP case (see Fig. S.3), and so the entirety of the improvement in SNR is due to suppressed noise in the interferometer's output. Such an improvement in SNR would translate into a suppression of readout error rate that is due to the finite SNR by a factor of 5 when starting out with an error rate of 1% with coherent light, which is normally achievable in superconducting qubit systems.

Outside this range of phases, readout with displaced two-mode squeezed vacuum has a lower SNR than with coherent light due to one or both of the two qubit states having a substantially higher noise than CS+PP readout. We also note that the improvement in SNR does not increase monotonically with squeezing strength; it reaches maximum for entangler gain between 1.5 dB and 2.5 dB, then decreases at higher entangler gain. There are two major reasons for this behavior of the SNR. First, photon loss inside the two-mode squeezed light interferometer limits the maximum amount of entanglement/noise reduction which can be achieved. Second, as we turn up the gain of the entangler JPC, it is more likely to saturate the analyzer JPC and cause its gain to drop and its amplification process to be less ideal, which reduces SNR. This effect is responsible for the drop of SNR for entangler gain of 4 dB shown in Fig. 4. [31, 32].

D. Quantum efficiency of a TMSL measurement

Another important figure-of-merit of a quantum measurement is its efficiency, which determines the fraction of information of the system being measured which is obtained by the observer, rather than lost to all other potential observers[1, 12, 33, 34]. Readout fidelity scales exponentially with measurement efficiency, and thus it plays a vital role in experiments which requires fast and high fidelity measurements, such as feedback control in quantum error correction [35].

In our experiment, the quantum efficiency η of our qubit measurement is determined by analyzing its back-action on the qubit with a weak measurement protocol established in Ref. [[12]]. This protocol provides a self-calibrated way of determining the overall efficiency of a measurement system. As there is no well established theory for weak measurement back-action with our TMS interferometer, we focus our study on two special cases where it most closely resembles the coherent light measurement; the 'TMS High' and 'TMS Low' cases shown in Fig. 3(a) where the output noise power is independent of the qubit state, and the interferometer's output resembles CS + PP readout with unusual noise values.

In Fig. 5 we summarize the results of the back-action experiments with coherent light and displaced two-mode squeezed vacuum ($G_e = 0.5$ dB). Fig. 5(a) shows the conditional x and y components of the qubit state Bloch vector for measurement results that have zero in-phase component ($I = 0$) of coherent light readout. In CS + PP readout, the x- and y-component of the qubit receive a purely quantum stochastic back-action due to the knowledge gained by the experimenter from the Q-component of the readout pulse. This effect can also be present in readout with coherent states plus phase-sensitive amplification (CS+PS). In CS+PS readout, the choice of amplified quadrature can shift from granting the observer only I-quadrature information (which we would usually call an optimal readout quadrature), and correspondingly maximal z-back action and no effect on the qubit's x- and y-components. By rotating the phase of the amplifier by 90°, we can reverse the situation, and produce only

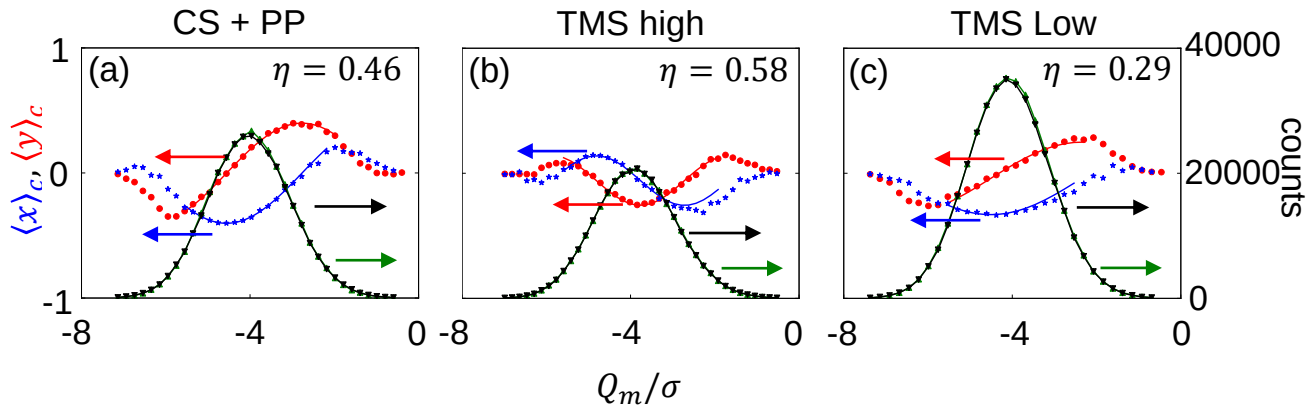

FIG. 5. **Quantum efficiency obtained by analyzing the back-action of weak measurements** Tomography data for x and y (blue stars and red dots) components of the qubit Bloch vector after we apply a weak measurement (see supplementary for details) are plotted against the left axis. The counts observed for each x and y tomography data points are shown with black down pointing triangle and green up pointing triangle, plotted against the right axis. The data is recorded for coherent light as well as displaced two-mode squeezed vacuum at relative pump phase point such that the ground and excited state qubit has the same noise level. Data is then fitted to the theory model for coherent light [12]. The measurement strength is adjusted such that all the measurements have the same SNR. The efficiency value obtained for each point is shown as well. The η is the quantum efficiency extracted from the fitting model . A surprisingly low quantum efficiency is observed when the system has less output noise level.

stochastic phase back-action[33, 36]. For CS + PP readout, these two back-actions are equal in amplitude, as the amplifier favors neither quadrature. The amplitude and frequency of the x and y-component oscillation, on the other hand, is determined by both the measurement strength and the efficiency of the measurement system. Therefore, by fitting this set of data, we can obtain the self-calibrated measurement strength and the overall efficiency of the measurement setup (see Supplemental for detailed procedure). From the data shown in Fig. 5(a), we obtain a overall efficiency of $\eta = 0.46$ for the coherent light readout method which sets the base line of our system. By accounting for the known loss in coherence due to T_2 process, we can also calculate a corrected efficiency of $\eta_{cor} = 0.52$.

Figure 5(b) and (c) show the results of applying the same protocol for displaced two-mode squeezed vacuum readout at the 'TMS High' and 'TMS Low' matched noise points, respectively. We have adjusted the drive amplitudes to match all three measurement types classical SNR (and correspondingly their z-component back-action, see Fig. S.7). However, the data clearly show that both the oscillation frequency and amplitude of the x- and y- components are very different from the CS + PP case, which indicates that the back-action strength and measurement efficiency are very different. From the same fitting, we obtain an efficiency of 0.58 at the displaced two-mode squeezed vacuum readout at the 'TMS High' point, and 0.29 at the 'TMS Low' point. One cause for this effect which we must rule out is that different TMS settings produce larger and smaller noise compared to the fixed contribution of the output chain following the analyzer JPC. As shown in Fig. S.8, even if we vary the relative noise contributed by the analyzer and the output chain, the known changes in output noise cannot explain simultaneously explain both the TMS High and Low results. Instead, it appears that the TMS readout behaves somewhat analogously to readout with a phase-sensitive amplifier, enhancing measurement SNR/z back-action at the TMS Low match point at the cost of rendering the x- and y-back action more sensitive to degradation by losses or added noise (and thus lowering the apparent efficiency in our imperfect apparatus). Interestingly, the TMS High match point, which represents a substantially *worse* SNR also allows the qubit's phase back-action to be more faithfully reported to an observer, even in the presence of loss and inefficiency.

IV. CONCLUSIONS AND OUTLOOK

In this work, we have demonstrated a new scheme for interferometric readout of a superconducting qubit with displaced two-mode squeezed vacuum and phase preservation amplification. In this readout scheme, we can increase the SNR of projective readout by suppressing the noise output of our amplifier below the usual Cave's limit for an amplifier fed with unsqueezed vacuum. In our experiment, we have achieved a 44% improvement in power SNR compared to conventional coherent light plus phase-preserving amplification readout. This improvement in SNR will result in a suppression of readout infidelity by

a factor of 5, if one starts with a 1% error rate in coherent light readout, with even greater improvements at higher base fidelities.

A still more interesting result emerges as we investigate the quantum readout efficiency of our TMS interferometer using weak measurements at points where the noise output is the same for both qubit states. These data show that there are important effects on the ratio between z back-action and the concomitant qubit phase back-action of this measurement process relative to other known readout schemes. It appears that the increase in SNR at the 'TMS Low' match point comes at the cost of reducing the trackability of phase back-action. Conversely, at the 'TMS High' match point this phase trackability is enhanced. Although we rule out post-interferometer noise as the source of this effect, more theoretical work is needed to understand the role of inefficiencies inside the interferometer due to imperfect squeezing/amplification and losses in the interferometer arms. This limitation notwithstanding, the fact that the 'TMS High' match point gives desirable quantum properties at a point which deliberately degrades SNR and fidelity of projective measurement should encourage exploration of measurement methods which are not just the quantum analogs of good classical measurement schemes.

Finally, while tracking a single qubit's phase during measurement is not of direct value for single qubit measurements in quantum computing, measurement-based entanglement is a vital component of many error-correction schemes in quantum information, and in these schemes[22, 23, 25], maintaining/tracking two qubit phase coherence during a high-fidelity measurement is vital. Our current experiment can be readily extended to two-qubit entanglement[25] by adding a second qubit on the lower arm, and we expect the ability to rebalance measurement strength and phase trackability *in-situ* to give crucial tolerance for losses and inefficiencies which currently limit these experiments.

V. ACKNOWLEDGMENTS

We acknowledge helpful discussions with S. Barzanjeh, Chenxu Liu, and David Pekker. This work was supported by the Army Research Office under Grants No. W911NF15-1-0397 and W911NF-18-1-0144, by NSF Grant No. PIRE-1743717 and by the Charles E. Kaufman Foundation of the Pittsburgh Foundation. The views and conclusions contained in this document are those of the authors and should not be interpreted as representing the official policies, either expressed or implied, of the Army Research Office or the US Government. The US Government is authorized to reproduce and distribute reprints for government purposes notwithstanding any copyright notation herein.

VI. SUPPLEMENTARY INFORMATION

A. Cryogenic Microwave Setup

The experiment is cooled down to around 20 mK on the base stage of a dilution refrigerator. The cryogenic microwave setup is shown in Fig. S.1. Fridge input lines carrying signals from room temperature to the system are attenuated and filtered with homemade lossy Eccosorb filters. Room temperature electronics, which include microwave generators, IQ mixers and an arbitrary waveform generator, are used to produce microwave pulses to drive the qubit and cavity. Both the qubit and cavity drives are sent into the system through the qubit-cavity input line, which connects to the weak port of the cavity. The JPCs are pumped with Keysight microwave generator. The output signal from the TMS interferometer is amplified by a chain of low noise cryogenic and room temperature amplifiers before been down-converted, digitized and demodulated with a room-temperature reference copy.

B. Sample parameters

The cavity in our experiment is a 3D aluminum coaxial post cavity with a resonance frequency of $\omega_c/2\pi = 7.447$ GHz, coupling quality factors of $Q_{strong} = 752$ on the strong port, and $Q_{weak} \sim 1,000,000$ on the weak port. Therefore, the cavity linewidth seen from the strong port is $\kappa/2\pi = 9.9$ MHz. The superconducting qubit is a 3D transmon qubit made by commonly used Dolan bridge technique with ground to excited state transition frequency of $\omega_{ge}/2\pi = 4.102$ GHz, anharmonicity $\alpha = 180$ MHz, and a qubit-cavity dispersive coupling strength of $\chi/2\pi = 2.2$ MHz . This qubit has a T_1 of 18.2 μs, and T_{2R} of 4.4 μs (T_{2E} is 4.6 μs). The cavity is placed in an aluminum shield that is inside a μ-metal cryoperm shield. The whole system is wrapped in mylar.

C. Gain interference in TMS light interferometer

The input and output mode (a and b) of a phase-preserving amplifier (e.g a JPC) can be related by the scattering relations:

$$a_{out} = S^\dagger a_{in} S = \cosh(r) a_{in} + e^{i\phi_p} \sinh(r) b_{in}^\dagger \quad \text{(S.1)}$$

$$b_{out}^\dagger = S^\dagger b_{in}^\dagger S = \cosh(r) b_{in}^\dagger + e^{-i\phi_p} \sinh(r) a_{in} \quad \text{(S.2)}$$

When two identical JPCs are connected with their signal and idler ports respectively, it is straightforward to calculate the scattering parameters for the combined system using the equations above twice. For example, the transmission gain from the signal port of the 'entangler' JPC to the signal port of the 'analyzer' JPC S_{aa} can be written as:

$$S_{aa} = \cosh(r_E)\cosh(r_A) + e^{i\Delta\phi} \sinh(r_E)\sinh(r_A) \quad \text{(S.3)}$$

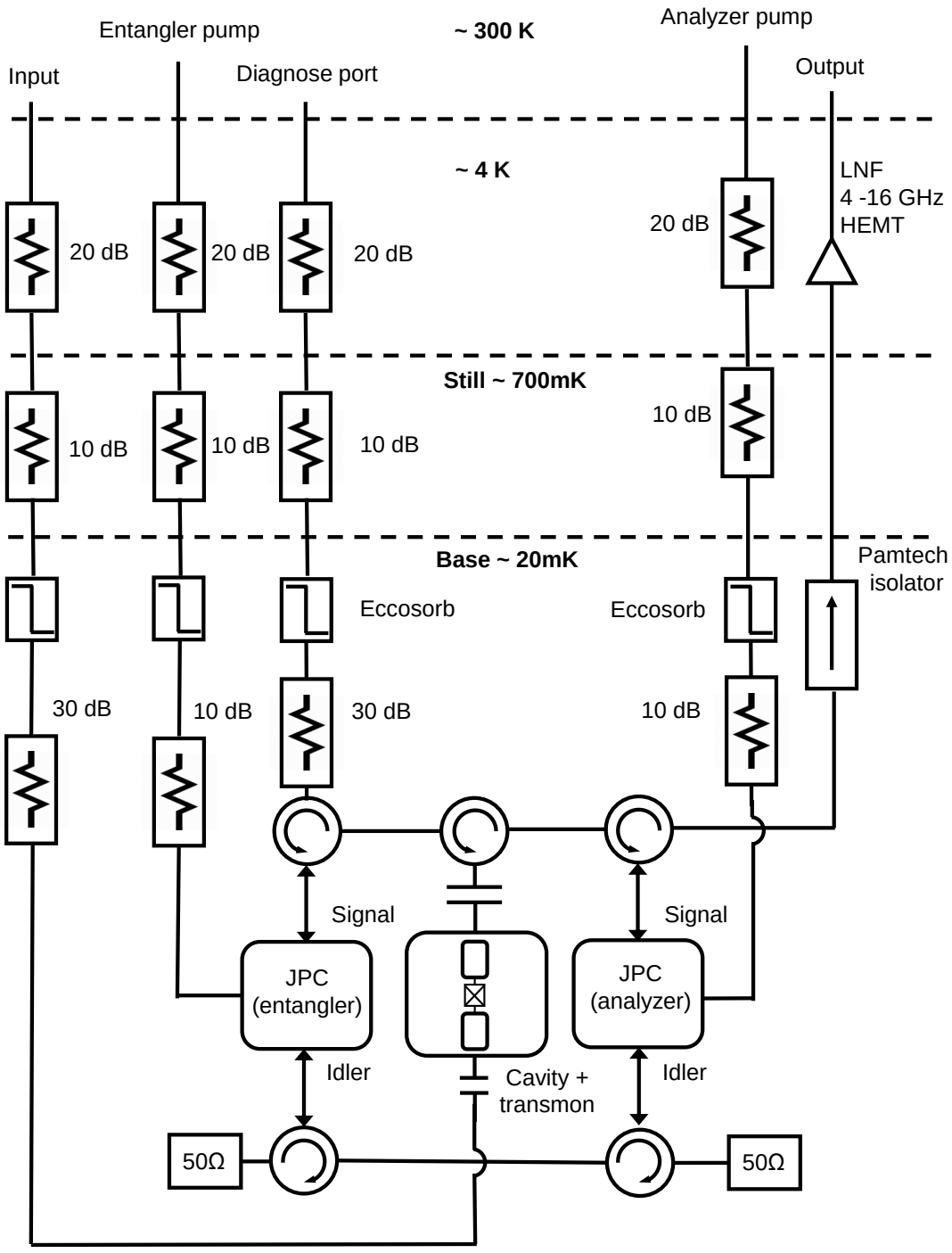

FIG. S.1. **Wiring diagram of the cryogenic microwave measurement setup.**

where we can see the amplitude of S_{aa} will vary with the relative pump phase $\Delta\phi$. Especially, when two JPCs has a matched gain ($r_E = r_A = r$) and a relative pump phase difference of π, the total gain of the system will become $\cosh^2(r) - \sinh^2(r) = 1$, indicating that the output signal power will be the same as the input signal. In the ideal case, when there is no loss and no added noise inside the interferometer, the output noise will just

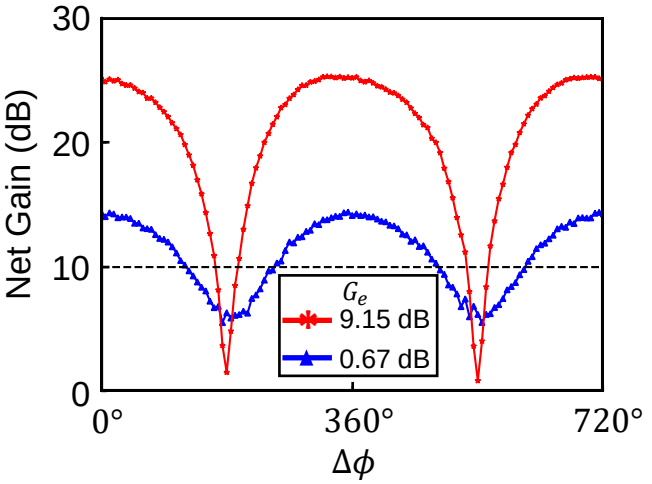

FIG. S.2. **Transmission measurement of the S parameter S_{aa} of the TMS interferometer as a function of the relative pump phase**. The gain of the analyzer JPC, G_a, is fixed to be 10 dB during the measurement (to avoid gain saturation for large entangler gain settings) as shown by the black dashed line. The blue triangle and red star trace corresponds to the different gain of the entangler JPC.

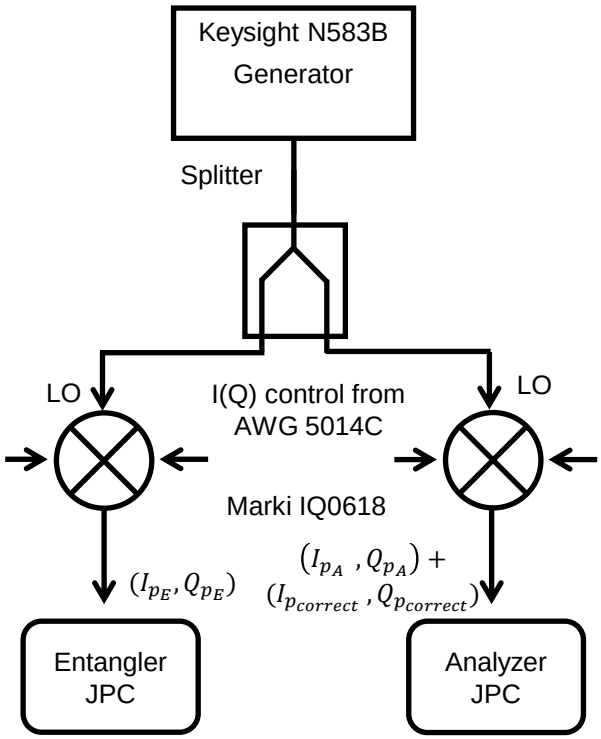

FIG. S.3. **Wiring diagram of room temperature setup for canceling the pump leakage.** The output of a single generator (Keysight N583B) is split and fed to two I/Q mixers which control the two JPC pumps. The Signal applied to the analyzer JPC is the sum of the desired pump and a correction designed to cancel leakage due to the entangler JPC pump. The use of a single generator has the additional benefit of stabilizing the relative phase of the two pumps, as a drift in phase of the generator affects both pumps equally.

be the uncorrelated vacuum noise present at the input of the interferometer. This scattering parameter is measured using a vector network analyzer as a function of the relative pump phase for a fixed analyzer JPC gain of $G_a = 10$ dB and different entangler JPC gains.

Fig S.2 shows data for $G_e = 0.67$ dB and 9.15 dB. By fitting these data with a modified version of Eq. S.3 which includes losses on both arms [19], we can extract the ratio of the transmission efficiencies of the upper and lower arms, which is found to be 0.9. We believe this imbalance in transmission is mostly due to the insertion loss of the extra circulator on the upper arm that connects to the qubit-cavity system. Given the stated loss of 0.2 dB per pass in the circulator, this would give 0.4 dB (transmission coefficient of 0.91) of additional loss on the upper arm, which is consistent with the loss ratio inferred from our data.

D. Pump leakage cancellation

Due the design of our JPC, applied pump tones preferentially leave from the signal and idler ports. Similarly, a pump tone can enter a JPC through its signal and idler ports (though in practice we apply pump tones only to the pump port). Thus, in our experiment, a fraction of the pump signal from the first JPC (entangler) always leaks into the second JPC (analyzer) through the arms of the interferometer. The reverse process is also possible, depending on the directionality of our interferometer at the pump frequency. Given that the two JPCs are biased so that their mode frequencies are matched and the second JPC is operated in the high gain (20 dB) regime, this pump leakage can cause large gain variation on the second JPC (gain variation as large as 15 dB was observed).

To eliminate this unwanted effect, we deliver the pump signals to the JPCs through a circuit shown in Fig. S.3 similar to the one used in Ref. [19]. In this circuit, the entangler pump is split and fed to two I/Q mixers which provide both JPC pumps. The analyzer's pump signal is a combination of a the desired analyzer pump and a phase and amplitude shifted copy of the entangler pump which cancels its leakage in the analyzer JPC. Experimentally, we nulled the leakage by varying the analyzer pump phase and identifying the correction factor where analyzer gain is insensitive to the presence or absence of the entangler pump. Another way of eliminating the pump leakage to the analyzer could be to add low-pass filters on both arms of the interferometer. However, this would introduce additional loss to the interferometer and degrade its performance. Therefore, we chose the active

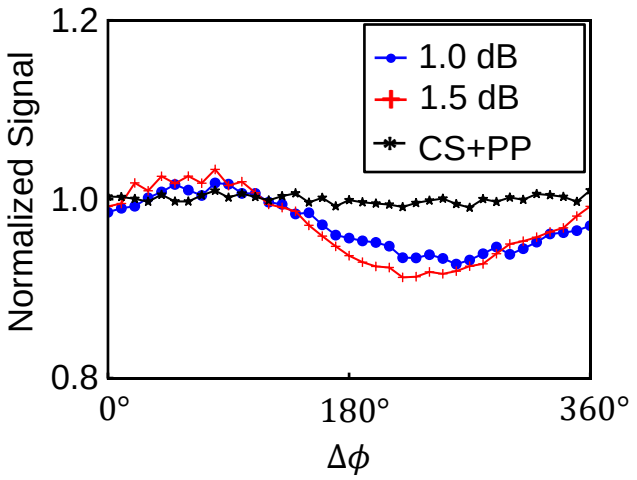

FIG. S.4. **Normalized signal strength of qubit readout with coherent light and displaced two-mode squeezed vacuum.** The strength of the signals are normalized by the average signal strength of the coherent light readout (CS + PP). Data shown here are for entangler gain $G_e = 1.0$ dB (blue dot), 1.5 dB (red cross) and 0 dB (CS + PP) (black star). The analyzer gain is kept constant at $G_a = 20$ dB.

method described here. More, to prove that this effect is due entirely to pump leakage, and not two-mode squeezing effects in the interferometer, we verified the presence of pump leakage and our cancellation scheme with the up-stream, entangler JPC tuned far away in frequency with flux.

To quantify how well the cancellation process works, we measured the output signal strength as a function of the relative pump phase for coherent light readout (CS+PP), which should have no pump variation, and displaced two-mode squeezed vacuum readout with the same cavity drive strength. Fig. S.4 shows the output signal strength normalized with respect to the average output signal strength of coherent light readout. For displaced two-mode squeezed vacuum readout, the output signal strength varies at most by -8%, which corresponds to a variation of 0.35 dB of the 20 dB gain of the analyzer. Note that this shift is negative, and decreases our SNR, so that the net observed enhancement in readout SNR is entirely due to a reduction in output noise and even larger than the overall SNR improvement suggests.

E. Back action of weak measurement

The quantum efficiency of the system for CS + PP readout is obtained by analyzing the back action of a weak measurement applied to the quit with a protocol established in Ref. [12]. To analyze the back action of a measurement, we use a pulse sequence shown in Fig. S.5.

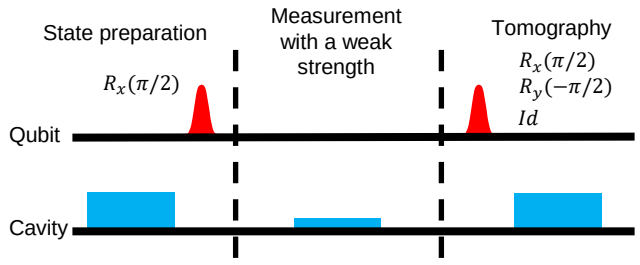

FIG. S.5. **Pulse sequence for quantifying measurement back action.** This pulse sequence consists three stages of qubit and cavity manipulation. The first stage is state preparation, during which the qubit is first projected to the state $|g\rangle$ by a strong measurement (blue box) and post-selection, and then rotated to the state $(|g\rangle + i\,|e\rangle)/\sqrt{2}$ by a $R_x(\pi/2)$ pulse (red Gaussian). The second stage is weak measurement, during which the qubit state is measured by a weak measurement pulse (thin blue box) and an outcome (I_m, Q_m) is recorded. In the third and final stage a qubit state tomography is performed by a combination of qubit rotation pulses (red Gaussian) $R_x(\pi/2)$, $R_y(-\pi/2)$ or Id (no pulse) and a strong measurement (blue box) pulse.

This pulse sequence begins with a strong measurement whose outcomes are post-selected to make sure that qubit always starts in $|g\rangle$. Next, a $R_x(\pi/2)$ pulse is applied to the qubit to rotate its state to $(|g\rangle + i\,|e\rangle)/\sqrt{2}$ $(Y = +1)$. Then, a weak measurement is performed by sending a pulse through the cavity which gives a measurement outcome (I_m, Q_m). Finally, to correlate the final state of the qubit with the outcome, a full qubit state tomography is performed by applying one of the three qubit rotation pulses, $R_x(\pi/2)$, $R_y(-\pi/2)$ and Id, and a strong measurement pulse which give the x, y and z components of the qubit Bloch vector, respectively.

Figure S.6(a) shows the data of the qubit state tomography for weak measurements with coherent light (top row). Each pixel of the 2D histograms contains the average value of all tomography measurement results of the x, y and z components of the qubit Bloch vector conditioned on receiving the (I_m, Q_m) value of that pixel from the weak measurement, which we refer to as the conditional tomography outcomes $\langle(x, y, z)\rangle_c$. According to the theory for coherent light[12, 37], the following relations describe the measurement-dependent back-action on the initial qubit state:

$$x_f^{\eta}(I_m, Q_m) = \mathrm{sech}\left(\frac{I_m \bar{I}_m}{\sigma^2}\right) \times \sin\left(\frac{Q_m \bar{I}_m}{\sigma^2} + \frac{\bar{Q}_m \bar{I}_m}{\sigma^2}\left(\frac{1-\eta}{\eta}\right)\right) \times e^{-\frac{\bar{I}_m^2}{\sigma^2}\left(\frac{1-\eta}{\eta}\right)} \tag{S.4}$$

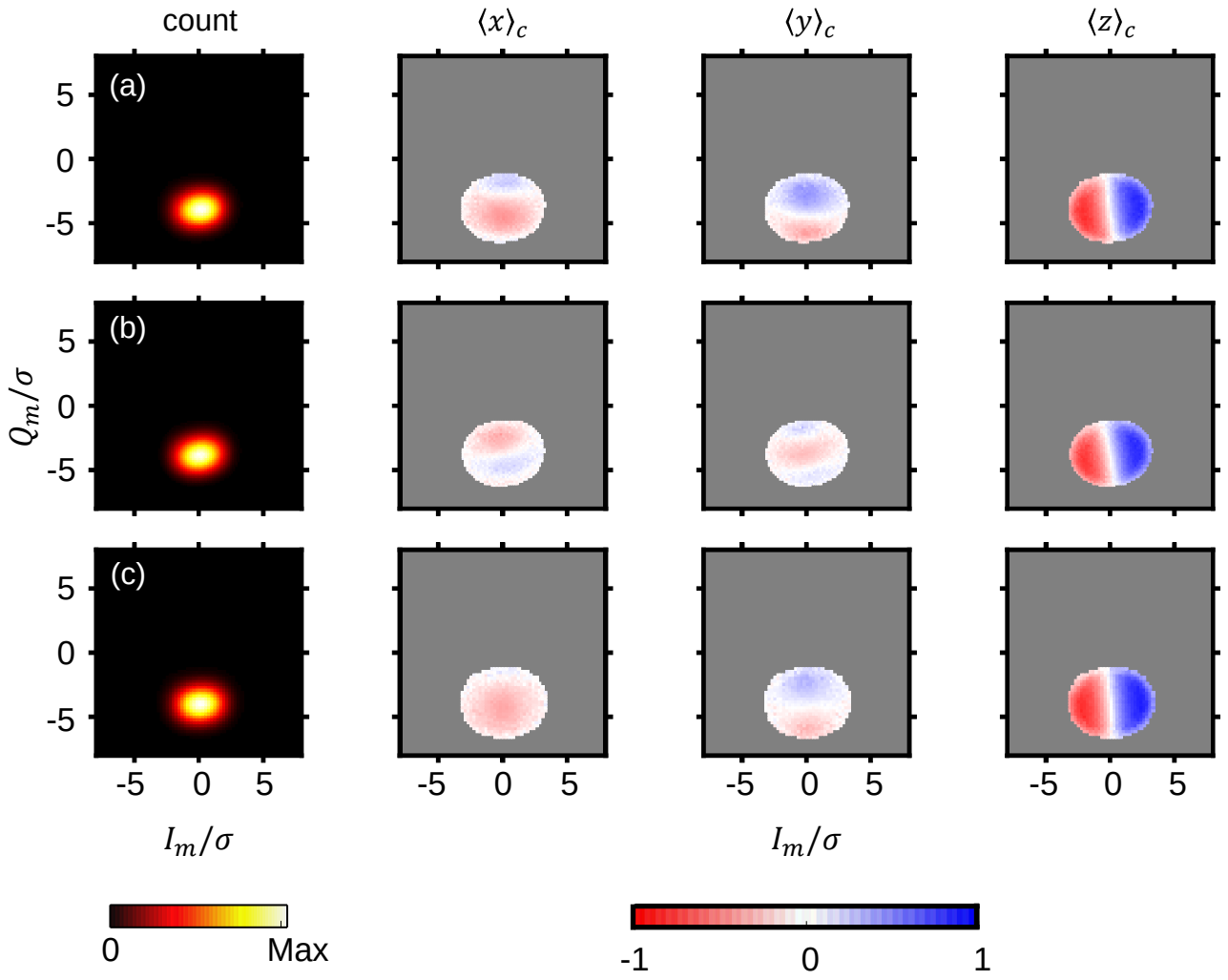

FIG. S.6. **Experiment data for back action of weak measurement.** Results are shown for the back action of the weak measurement for coherent light (a) and displaced two-mode squeezed vacuum at high(b) and low(c) noise level match point. In all three cases, the strength of the weak measurement is $\bar{I}_m/\sigma = 0.66$. The leftmost column shows the 2D histograms of scaled measurement outcomes recorded during the weak measurements. The right three columns are the conditional tomography data for $\langle x\rangle$, $\langle y\rangle$ and $\langle z\rangle$ component versus the associated $(I_m/\sigma, Q_m/\sigma)$ bin. The value in each bin is the average of all tomography data associated with that (I_m, Q_m) value.

$$y_f^\eta(I_m, Q_m) = \mathrm{sech}(\frac{I_m\bar{I}_m}{\sigma^2}) \times \cos(\frac{Q_m\bar{I}_m}{\sigma^2} + \frac{\bar{Q}_m\bar{I}_m}{\sigma^2}(\frac{1-\eta}{\eta})) \times e^{-\frac{\bar{I}_m^2}{\sigma^2}(\frac{1-\eta}{\eta})} \tag{S.5}$$

$$z_f^\eta(I_m, Q_m) = \tanh(\frac{I_m\bar{I}_m}{\sigma^2}). \tag{S.6}$$

Here $(\bar{I}_m, \bar{Q}_m)$ and σ are the center and standard deviation of the outcome distributions of the weak measurement and η is the quantum efficiency of the system. Data shown in Fig. 5 are line cuts of the x and y tomography data along $I_m = 0$, where there is no z back-action. Oscillation in $\langle x\rangle_c$ and $\langle y\rangle_c$ shows the stochastic phase back action. By fitting the line cuts shown in Fig. 5 with the above formulae, we obtained the overall efficiency for different readout methods reported in the paper by comparing the frequency and amplitude of the oscillations.

For TMSL High and Low matched readout, we can use this protocol to probe the measurement back-action. While we lack a full theory for this back-action, we are encouraged by the overall outcomes resemblance to 'CS+PP with altered noise'. Indeed, in Fig. S.6(b), (c) we see a close resemblance of the data to CS + PP readout. To compensate for the varying SNR/histogram separation in these three cases, the strength of the cavity drive is varied such that the separation of the two states in the histograms is the same, so that $\bar{I}_m/\sigma$ match. This

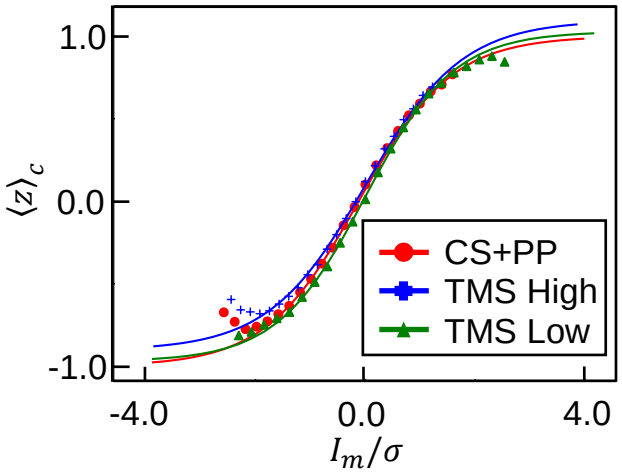

FIG. S.7. **Experiment data for z-axis back action of weak measurement.** Tomography data for z-component of the qubit Bloch vector along $Q_m = -4$ of the 2D histograms shown in Fig. S.6. Different color indicates the case for CS + PP, TMS high match and TMS low match, respectively.

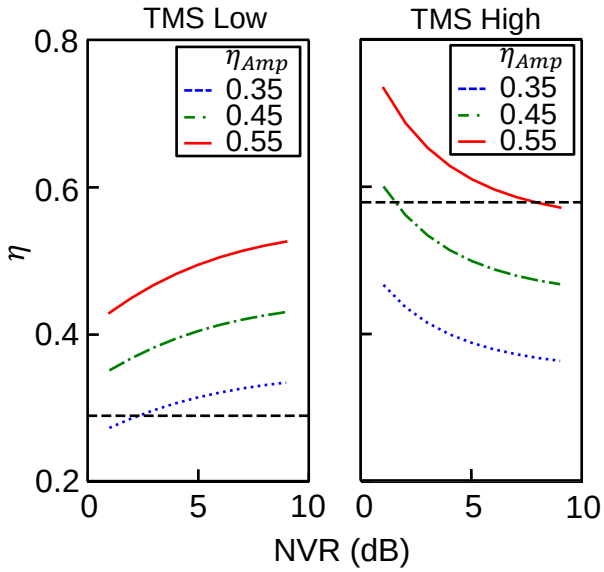

FIG. S.8. **Calculated overall efficiency of our measurement system for displaced two-mode squeezed vacuum as a function of NVR for different analyzer JPC/TMS interferometer efficiency.** Overall efficiency of the system vs NVR at the 'TMS Low' and 'TMS High' matched points for different amplifier efficiency $\eta_{\rm Amp} = 0.35$ (blue dash line), 0.45 (green dotted line) and 0.55 (red line). The black dash lines show the value of efficiency obtained from the weak measurement protocol.

should result in a semi-classical z back-action which is indistinguishable for all three case. As in shown in Fig. S.7 in which we plot a line cut of $\langle z \rangle_c$ through $Q_m = -4$, this is indeed the case. Given that the data do not vary with Q_m, we could also have averaged all data along Q_m to achieve a similar result. However, the x and y back-action, although similar in form, show very different apparent strength and efficiency, as discussed in the main text.

F. Noise visibility ratio and quantum efficiency

In this section, we will show that the observed large changes in quantum efficiency of the three readout methods *can not* be explained by changes in the ratio of output noise of the TMS interferometer and the classical noise from the output chain.

The overall measurement efficiency of the system extracted from the weak measurement protocol can be expressed as:

$$\eta = \eta_{\rm Amp}\ \eta_{\rm out}, \tag{S.7}$$

where η_{Amp} is the efficiency of the system before HEMT (qubit-cavity and JPC/TMS interferometer), $\eta_{\rm out}$ is the efficiency of the output chain after the analyzer JPC which is dominated by the efficiency of the HEMT amplifier. The efficiency of the output chain, $\eta_{\rm out}$, can be expressed as:

$$\eta_{\rm out} = \frac{N_{\rm Amp}}{N_{\rm Amp} + N_{\rm out}}. \tag{S.8}$$

where $N_{\rm Amp}$ is the output noise power of the analyzer JPC, $N_{\rm out}$ is the added noise power of the output chain referred back to the input of the HEMT. An easily measurable quantity in the lab that is closely related to $\eta_{\rm out}$ is the noise-visibility-ratio (NVR),

$$NVR = \frac{N_{\rm Amp} + N_{\rm out}}{N_{\rm out}}. \tag{S.9}$$

It is easy to see:

$$\eta_{\rm out} = 1 - \frac{1}{NVR}. \tag{S.10}$$

In our experiment, the NVR is typically 7 dB when the analyzer JPC is operated at 20 dB gain. Therefore, for coherent light readout, given $\eta = 0.46$ extracted from the weak measurement, we have $\eta_{Amp} = 0.58$ for our system.

Now consider the case of the displaced two-mode squeezed vacuum (TMS). Even though we did not measure the its NVR directly, we can calculate it based on the NVR of coherent light and the noise suppression/enhancement shown in Fig. 3. The NVR for TMS at the high (H) and low (L) match points can be expressed as

$$NVR^{H/L}_{TMS} = 1 + \frac{N^{H/L}_{TMS}}{N_{\rm out}} = 1 + \frac{N_{CS}}{N_{\rm out}}(\frac{\sigma^{H/L}_{TMS}}{\sigma_{CS}})^2, \tag{S.11}$$

which is larger (smaller) at the high (low) match point than that of coherent light. Consequently, the efficiency

of the output chain ($\eta_{\rm out}$) will also be larger (smaller) than that of the coherent light readout.

If we assume the quantum efficiency of TMS interferometer is the same as that in the coherent light case, namely, $\eta_{Amp} = 0.58$, and a typical coherent light NVR, 7 dB, then given the $\frac{\sigma^H_{TMSL}}{\sigma_{CS}} = 1.21$ and $\frac{\sigma^L_{TMSL}}{\sigma_{CS}} = 0.86$, we can calculate the overall quantum efficiency of the system at the high and low σ match point. We get $\eta^H = 0.48 < \eta^H_{exp} = 0.58$ and $\eta^L = 0.42 > \eta^L_{exp} = 0.29$.

More generally, in Fig. S.8 we plot the overall efficiency as a function of NVR for different values of $\eta_{\rm Amp}$. It clearly shows that the measured efficiency at 'TMS Low' and 'TML High' match points requires, in addition to the changes in NVR, the analyzer JPC/TMS interferometer to have different quantum efficiencies which itself requires further studies.

[1] A. A. Clerk, M. H. Devoret, S. M. Girvin, F. Marquardt, and R. J. Schoelkopf, Reviews of Modern Physics **82**, 1155 (2010).

[2] A. Blais, R. S. Huang, A. Wallraff, S. M. Girvin, and R. J. Schoelkopf, Physical Review A - Atomic, Molecular, and Optical Physics **69**, 1 (2004).

[3] C. Macklin, K. OBrien, D. Hover, M. Schwartz, V. Bolkhovsky, X. Zhang, W. Oliver, and I. Siddiqi, Science **350**, 307 (2015).

[4] N. Bergeal, F. Schackert, M. Metcalfe, R. Vijay, V. E. Manucharyan, L. Frunzio, D. E. Prober, R. J. Schoelkopf, S. M. Girvin, and M. H. Devoret, Nature **465**, 64 (2010).

[5] N. Frattini, V. Sivak, A. Lingenfelter, S. Shankar, and M. Devoret, Physical Review Applied **10**, 054020 (2018).

[6] I. Siddiqi, R. Vijay, F. Pierre, C. Wilson, M. Metcalfe, C. Rigetti, L. Frunzio, and M. Devoret, Physical review letters **93**, 207002 (2004).

[7] C. M. Caves, K. S. Thorne, R. W. Drever, V. D. Sandberg, and M. Zimmermann, Reviews of Modern Physics **52**, 341 (1980).

[8] A. Wallraff, D. I. Schuster, A. Blais, L. Frunzio, J. Majer, M. H. Devoret, S. M. Girvin, and R. J. Schoelkopf, Physical Review Letters **95**, 1 (2005).

[9] J. Gambetta, A. Blais, D. I. Schuster, A. Wallraff, L. Frunzio, J. Majer, M. H. Devoret, S. M. Girvin, and R. J. Schoelkopf, Physical Review A **74**, 042318 (2006).

[10] T.-C. Chien, O. Lanes, C. Liu, X. Cao, P. Lu, S. Motz, G. Liu, D. Pekker, and M. Hatridge, Physical Review A **101**, 042336 (2020).

[11] R. Vijay, D. Slichter, and I. Siddiqi, Physical review letters **106**, 110502 (2011).

[12] M. Hatridge, S. Shankar, M. Mirrahimi, F. Schackert, K. Geerlings, T. Brecht, K. M. Sliwa, B. Abdo, L. Frunzio, S. M. Girvin, R. J. Schoelkopf, and M. H. Devoret, Science **339**, 178 (2013).

[13] C. M. Caves, Physical Review D **23**, 1693 (1981).

[14] S. Barzanjeh, D. P. Divincenzo, and B. M. Terhal, Physical Review B - Condensed Matter and Materials Physics **90** (2014), 10.1103/PhysRevB.90.134515.

[15] B. Yurke, S. L. McCall, and J. R. Klauder, Physical Review A **33**, 4033 (1986).

[16] C. M. Caves, Physical Review D **26**, 1817 (1982).

[17] H. Zheng, M. Silveri, R. Brierley, S. Girvin, and K. Lehnert, arXiv preprint arXiv:1607.02529 (2016).

[18] N. Bergeal, R. Vijay, V. E. Manucharyan, I. Siddiqi, R. J. Schoelkopf, S. M. Girvin, and M. H. Devoret, Nature Physics **6**, 296 (2010).

[19] E. Flurin, N. Roch, F. Mallet, M. H. Devoret, and B. Huard, Physical Review Letters **109**, 1 (2012).

[20] C. M. Caves, J. Combes, Z. Jiang, and S. Pandey, Physical Review A **86**, 063802 (2012).

[21] A. Eddins, S. Schreppler, D. M. Toyli, L. S. Martin, S. Hacohen-Gourgy, L. C. Govia, H. Ribeiro, A. A. Clerk, and I. Siddiqi, Physical Review Letters **120**, 40505 (2018).

[22] N. Roch, M. E. Schwartz, F. Motzoi, C. Macklin, R. Vijay, A. W. Eddins, A. N. Korotkov, K. B. Whaley, M. Sarovar, and I. Siddiqi, Physical review letters **112**, 170501 (2014).

[23] C. Dickel, J. Wesdorp, N. Langford, S. Peiter, R. Sagastizabal, A. Bruno, B. Criger, F. Motzoi, and L. DiCarlo, Physical Review B **97**, 064508 (2018).

[24] A. Narla, S. Shankar, M. Hatridge, Z. Leghtas, K. M. Sliwa, E. Zalys-Geller, S. O. Mundhada, W. Pfaff, L. Frunzio, R. J. Schoelkopf, and M. H. Devoret, Physical Review X **6** (2016), 10.1103/physrevx.6.031036.

[25] M. Silveri, E. Zalys-Geller, M. Hatridge, Z. Leghtas, M. H. Devoret, and S. M. Girvin, Physical Review A **93**, 1 (2016).

[26] C. M. Caves and B. L. Schumaker, Physical Review A **31**, 3068 (1985).

[27] C. C. Gerry, Journal of Modern Optics **42**, 585 (1995).

[28] R. Loudon and P. L. Knight, Journal of Modern Optics **34**, 709 (1987), arXiv:arXiv:1401.4118v2.

[29] N. Bergeal, F. Schackert, L. Frunzio, and M. H. Devoret, Physical Review Letters **108**, 1 (2012).

[30] A. Wallraff, D. I. Schuster, A. Blais, L. Frunzio, R.-S. Huang, J. Majer, S. Kumar, S. M. Girvin, and R. J. Schoelkopf, Nature **431**, 162 (2004).

[31] T. Walter, P. Kurpiers, S. Gasparinetti, P. Magnard, A. Potočnik, Y. Salathé, M. Pechal, M. Mondal, M. Oppliger, C. Eichler, *et al.*, Physical Review Applied **7**, 054020 (2017).

[32] J. Heinsoo, C. K. Andersen, A. Remm, S. Krinner, T. Walter, Y. Salathé, S. Gasparinetti, J.-C. Besse, A. Potočnik, A. Wallraff, *et al.*, Physical Review Applied **10**, 034040 (2018).

[33] A. N. Korotkov, Phys. Rev. A **94**, 042326 (2016).

[34] K. Murch, S. Weber, C. Macklin, and I. Siddiqi, Nature **502**, 211 (2013).

[35] S. Shankar, M. Hatridge, Z. Leghtas, K. M. Sliwa, A. Narla, U. Vool, S. M. Girvin, L. Frunzio, M. Mirrahimi, and M. H. Devoret, Nature **504**, 419 (2013).

[36] K. Sliwa, *Improving the quality of Heisenberg back-action of qubit measurements made with parametric amplifiers* (Yale University, 2016).

[37] A. Sarlette and P. Rouchon, Journal of Mathematical Physics **58**, 062106 (2017).